Distinct and Dynamic Distributions of Multiple Elements and Their Species in the Rice Rhizosphere

Zhao-Feng Yuan
Xi'an Jiaotong-Liverpool University
Williamson Gustave
Xi'an Jiaotong-Liverpool University
Syed Tahir Ata-Ul-Karim
The University of Tokyo
Jonathan Bridge
Sheffield Hallam University
Raju Sekar
Xi'an Jiaotong-Liverpool University
Fuyuan Liu
Xi'an Jiaotong-Liverpool University
Zheng Chen (zheng.chen@xjtlu.edu.cn)
Xi'an Jiaotong-Liverpool University https://orcid.org/0000-0002-1184-3682

Research Article

Keywords: rice rhizosphere, spatiotemporal, multiple elements, arsenic, cadmium

Posted Date: May 13th, 2021

DOI: https://doi.org/10.21203/rs.3.rs-497239/v1

Version of Record: A version of this preprint was published at Plant and Soil on August 19th, 2021. See the published version at https://doi.org/10.1007/s11104-021-05100-x.

Abstract

Aims

The biogeochemical cycles of elements from soils to plants are mainly governed by their rhizosphere processes. Understanding these processes is challenging and remains largely unresolved due to the complex interrelationships among different elements and due to a lack of appropriate techniques for simultaneous spatiotemporal monitoring.

Methods

This study employed an *In-situ* Porewater Iterative (IPI) sampler array (0-22 mm measurement distance every 1.7 mm, with a time interval of 3 to 10 days) to capture the *in situ* spatiotemporal dynamics of ten elements (Fe, Mn, As, P, S, Cr, Co, Zn, Sb and Cd) in the paddy rhizosphere to examine their covarying changes in time and space dimensions.

Results

The findings revealed that the solute-phase concentration of most elements, other than Sb and Cd, increased to a peak after 30 days of paddy soil flooding and then decreased. Additionally, Sb and Cd continuously decreased during flooding. Fe (-52%), Mn (-17%), P (-43%), Co (-11%), and As species (-74%) were substantially immobilized within a 10 mm zone around the roots, while Zn (28%) and Cd (41%) increased. The greater immobilization of As and re-mobilization of Cd, in the rhizosphere, are stimulated by biotic oxidation of arsenite to arsenate with root oxygen loss and the pH decrease, respectively.

Conclusions

Our study showed most sampled elements covaried with Fe both in time and space in the rhizosphere, but the elements are temporally and spatially determined by multiple biogeochemical processes in soils as well as exudates from plant roots.

Introduction

The ability of rice to adapt in order to grow under diverse conditions (aerobic and anaerobic) gives it a unique status among crops. This diversity results in differences in biogeochemical reactions that alter the interactions between soil chemistry and rice roots (Kuzyakov and Razavi 2019). Oxygen (O_2) in paddy soils under flooded conditions is rapidly consumed by microbes during the rice growth period, and the passive transportation of atmospheric O_2 through aerenchymatous tissues enables rice to withstand hypoxic conditions (Revsbech et al. 1999). O_2, other than that respired by rice roots, is released by roots as radial oxygen loss (ROL), which results in significant deposition of iron (Fe) in the rhizosphere after reacting with the abundant ferrous Fe ions (Fe^{2+}) in soil porewater (Chen et al. 2005). The microbial community, nutrient availability, pollutant mobility, and greenhouse gas emissions in paddy soils are

greatly influenced by alterations in rhizosphere characteristics as a consequence of ROL-induced oxidizing areas (Kuzyakov and Razavi 2019), which may extend approximately 10–25 mm from the root surface (Maisch et al. 2019). The elucidation of all indigenous processes occurring in the rice rhizosphere is imperative for improving soil and rice quality. However, a thorough description of these processes remains largely unresolved.

Rhizospheric processes are strongly influenced by the formation of Fe oxides around rice roots (i.e., Fe plaque) in paddy soils, owing to the diversified role of Fe plaque as a barrier (Chen et al. 2005; Martin et al. 2019) and/or facilitator (Richardson et al. 2009; Yin et al. 2020) of mineral uptake. The barrier effect is mainly due to the high affinity of Fe oxides, which have a high surface area and rich functional groups capable of binding with anions and cations (Hansel et al. 2001; Suda and Makino 2016). Many studies have reported that Fe plaques inhibit arsenic (As) (Chen et al. 2005), phosphorus (P) (Zhang et al. 1999), lead (Ma et al. 2012), copper (Ye et al. 2001), nickel (Ni) (Xu et al. 2015), and cadmium (Cd) (Liu et al. 2007) uptake by plants. However, the function of the Fe plaques may be reversed when other processes are involved. The coupling of Fe^{2+} oxidization with proton release leads to acidification of the rhizosphere (Kuzyakov and Razavi 2019; Maisch et al. 2019), which in turn enhances metal ion bioavailability through their desorption from solid minerals (Wang et al. 2019). Furthermore, in reducing paddy soils, sulfides (S(-II)) are produced by sulfate (S(VI))-reducing bacteria and form metal/metalloid S(-II) (Arsic et al. 2018; Borch et al. 2010; Pester et al. 2012). The S(-II) of metals/metalloids (e.g., copper, Cd, mercury, antimony (Sb) and As) are not readily available for plant uptake owing to their extremely low solubility. Sulfur (S)-oxidizing bacteria exposed to the ROL-inducing oxic rhizosphere use rich electron acceptors (Martin et al. 2019; Thomas et al. 2014), including O_2, nitrate and Fe oxides, to oxidize reducing S and remobilize the metals/metalloids. The rhizosphere acidification and release of root exudates tend to enhance metal/metalloid remobilization in the rhizosphere (Kuzyakov and Razavi 2019). Assessing element behaviors in the paddy rhizosphere is difficult due to complex interactions among elements that are dependent on the chemical nature, root functions, rhizosphere, and microbial activity of the elements. Consequently, it is plausible to speculate that different elements have different spatial distributions in the paddy rhizosphere, and a detailed examination of their distribution in the rhizosphere is required for an in-depth understanding of the processes occurring in the rice root-soil system.

The chemical gradients in the paddy rhizosphere swiftly change in time and space. The distribution of oxidized areas along the entire active roots has been evaluated by using electrochemical probes and planar optodes, but the highest O_2 concentrations were observed in the 2–4 mm region around the tips of young roots (Williams et al. 2014; Yin et al. 2020). In contrast, solute-phase Fe^{2+} exhibits an opposite trend to O_2, namely, Fe^{2+} is low on the root surface (Maisch et al. 2019). Fine mapping of trace elements in the paddy rhizosphere has rarely been investigated. A new hotspot of greatly enhanced fluxes of As, Pb and Fe(II) adjacent to rice root tips (within a few mm) using diffusive gradients in thin films (DGT) has been documented (Williams et al. 2014). However, the root tips have a weak impact on cobalt (Co), manganese (Mn), zinc (Zn), and Ni (Yin et al. 2020). DGT, despite being a very powerful tool for generating 2D spatial maps of elements, can only take a snapshot at a certain time interval. Conversely,

other soil solution samplers, such as microsuction cups, can be used for repeated measurements but cannot be used to map the chemical gradient (Brackin et al. 2017; Seeberg-Elverfeldt et al. 2005). To date, the measurements cannot probe the dynamics of the rhizosphere at a sufficient resolution; they are fixed (or limited) either in time or in space. Consequently, a detailed understanding of the spatiotemporal changes in elements in the paddy rhizosphere remains dubious due to the lack of appropriate techniques for mapping the dynamic distribution of elements in the paddy rhizosphere.

This study aimed to reveal the complex processes of soluble elements in the paddy rhizosphere by applying a tool called Rhizon profiler. The profiler was based on the In-*situ* Porewater Iterative (IPI) sampler developed by our group (Yuan et al. 2019), which can repeatedly collect porewater with ultralow disturbance of the soil matrix. Being coupled with ICP-MS or IC-ICP-MS (Yuan et al. 2019, 2021), this sampler can provide a two-dimensional (space and time) map of elements and/or their species in porewater across the paddy rhizosphere. The two dimensions of the Rhizon profilers are a spatial dimension (0–22 mm distance from the root bag surface) with a resolution of 1.7 mm and a time dimension with a resolution of 24 hours. This updated sampler can act as a powerful tool to identify hotspots and hot moments in the rhizosphere. This study focused on As and Cd due to their higher accumulation in rice grains and the health risk associated with their dietary intake. However, due to the presence of P, S, Zn, Fe, Mn, Cr, Co, and Sb in paddy soils (Eberle et al. 2020; Shaheen et al. 2014; Wan et al. 2019; Wang et al. 2019; Zhang et al. 1999), their potential association with As and Cd behaviors in flooded soils was also investigated in this study.

We hypothesized that (1) most elements in the paddy rhizosphere covary with Fe in time and space owing to the high adsorption capacity of Fe oxides and (2) the ROL-induced zone hosts distinct species distributions mediated by microbes. Four As species (arsenite (As(III)), arsenate (As(V)), monomethylarsonic acid (MMA), and dimethylarsinic acid (DMA)) are common in paddy soils (Guo et al. 2020; Kumarathilaka et al. 2018; Muehe et al. 2019). As(V) is reduced to As(III) when soils become reducing and is further methylated to DMA when anaerobic microorganisms possessing the capacity for As methylation thrive. The demethylation process driven by methanogens dominates under continuously decreasing Eh (Chen et al. 2019). The transformation of As species may actively occur in the paddy rhizosphere (Afroz et al. 2019). The availability of electron acceptors and donors makes the paddy rhizosphere a potential hotspot for the transformation of elemental species; however, sampling along the redox gradient in the rhizosphere has been a major challenge. This study endeavored to test these hypotheses with real contaminated paddy soils by profiling the elements outside the root bags of rice plants.

Materials And Methods

Experimental preparation

As-contaminated paddy soil was collected from Shaoguan (25°6'N, 113°38'E), China. The topsoil layer (0-20 cm) was sampled followed by wet sieving to remove stones and plant debris through a 1.0 mm

diameter sieve. The selected soil properties are depicted in Table S1. The rice hybrid Yliangyou-1 was sterilized and germinated following the method described in a previous report (Chen et al. 2012). The seedlings were grown in a Hoagland culture in a glass greenhouse from 30 March 2019 to 1 May 2019 (three-leaf stage) before being transplanted into the soils. The plants were grown in a glass greenhouse under natural light, and the temperature was set and controlled at 25/20 °C days/night controlled by an air conditioner.

Porewater sampling by Rhizon profilers

The IPI sampler used in this study shares the same design as in a recent report by our group (Yuan et al. 2021). The structure of an IPI sampler is shown in Fig. 1A. The IPI sampler includes three components: (1) the hollow fiber membrane tube (modified polyethersulfone, 20 nm pore size, inner × outer diameter × length = 1.0 mm × 1.7 mm × 35 mm, 27.5 μL, Motimo Membrane Technology Co., Ltd., Tianjin, China); (2) two pipes (PTFE, inner × outer diameter × length = 0.5 mm × 1.0 mm × 180 mm, 35 μL); and (3) two silicon caps (inner × outer diameter × depth × length = 1.0 mm × 2.0 mm × 10 mm × 20 mm). When the IPI sampler is deployed into solution or saturated soils, solutes around the hollow fiber membrane tube can diffuse through the membrane (Fig. 1A). The solution inside the tube is pumped out and collected when the diffusion reaches equilibrium (24 hours) (Yuan et al. 2019, 2021). During deployment, silicon caps are applied to seal the IPI sampler to avoid potential contamination (e.g., gasoline fumes) from the atmosphere. During each sampling event, a 27.5 μL liquid sample in the sampling tube was mixed with 70 μL ultrapure water in the pipes when they were pumped out from the sampler. This indicates that an approximately 100 μL porewater sample can be collected each time by the IPI sampler, with a dilution factor of 3.5.

Horizontally assembled IPI samplers were designed to measure a sampling zone across the rhizosphere at a sufficient resolution (mm level) (Fig. 1B). To achieve this, thirteen IPI samplers were horizontally assembled in a 3D printed holder (Fig. 1C). The IPI sampler array, i.e., the Rhizon profiler, after being combined with a nylon mesh bag (nominal pore size = 37 μm, height × width = 10 mm × 8 cm), is able to collect porewater *in situ* at a 0-22 mm distance from the root bag surface every 1.7 mm, and the rhizosphere soils can be destructively collected from a soil slot adjacent to the porewater samplers (Fig. 1C). When deploying the Rhizon profiler and root bag into the soils incubated in the pot in this study, well-mixed wet soils (3000 g; 100% moisture) were added into a black plastic bucket (inner diameter × height = 15-18 cm × 21 cm) with a soil depth of approximately 15 cm, and 600 g of the total 3000 g was enclosed in the root bag. The Rhizon profiler along with the root bag was buried at approximately 8 cm depth below the soil-water interface followed by the addition of ultrapure water to maintain a 3-5 cm overlying water depth during the experiment.

In situ multielement measurement across the rhizosphere

A pot experiment with three replicates was conducted with (treatment)/without (control) rice growing into the root bag (Fig. S1). Two seedlings were transplanted into each root bag of the treatment group upon the soil flooding. The pots were placed in a glass greenhouse at randomly selected locations. The

positions of the pots were switched every other day during the experiment to minimize the potential influence of the external environment. Porewater was sampled *in situ* across 0-22 mm from the root bag/surface by Rhizon profilers at days after paddy soil flooding (DAF) 0, 3, 8, 15, 24, 30 and 40 with or without rice growing in root bags. Multielement information in each 100 µL porewater sample was determined by the high-throughput analytical method developed by our group (Yuan et al. 2020). Total solute-phase Fe, Mn P, S, As, Cd, Sb, Cr, Co and Zn preserved with HCl were measured by inductively coupled plasma-mass spectrometry (ICP-MS, NexION 350X, PerkinElmer, Inc., Shelton, CT USA) with data only analysis. The $^{57}Fe^{+}$, $^{55}Mn^{+}$, $^{47}PO^{+}$, $^{48}SO^{+}$, $^{91}AsO^{+}$, $^{111}Cd^{+}$, $^{121}Sb^{+}$, $^{52}Cr^{+}$, $^{59}Co^{+}$ and $^{66}Zn^{+}$ counts were recorded in a dynamic reaction cell (DRC, O_2 as the reaction gas) or extended dynamic range (EDR) mode simultaneously. The sample taken at DAF 40, preserved with EDTA, was used to measure As [As(III), As(V), MMA, DMA] and S [S(VI), S(-II)] species by coupling ion chromatography (IC, Dionex ICS-1100, Thermo Scientific, USA) with ICP-MS using the NH_4HCO_3 mobile phase (20 mM, pH = 10) (Suzuki et al. 2009; Yuan et al. 2019). A spiked standard was tested after every 30 samples to assure data quality.

Plant and microbial analysis

Multiple elements in plant tissues and the microbial community in the rhizosphere were investigated at the jointing stage (DAF 40). The Rhizon profilers and root bags were retrieved from the soils after porewater sampling at DAF 40. The rice plants were removed from the root bags, and their roots were gently cleaned with ultrapure water. The fresh plants were separated into roots, stems and leaves, followed by oven-drying (60 °C) and freeze-drying (-85 °C) of subsamples for the subsequent determination of total elements and As species, respectively. Plant samples after oven-drying were weighed to measure the plant dry matter, followed by grinding and sieving through a 1.0 mm sieve for chemical analysis. A sample of 0.5 g was digested using a 1:1 mixture of concentrated HNO_3 and H_2O_2 (Gustave et al. 2019). The digested samples were filtered through a 0.45 µm cellulose filter and diluted with ultrapure water. The total Fe, Mn, P, S, As, Cd, Sb, Cr, Co and Zn were measured by ICP-MS. Freeze-dried ground samples (0.2 g) were extracted with a modified protein extraction solution (Quaghebeur et al. 2003). The extracted samples were filtered through a 0.45 µm pore size filter and measured by IC-ICP-MS. Spiked standards were tested to assure data quality.

Soils at 0-2 mm from the root bags (the soils were deposited within a slot on a Rhizon profiler, Fig. 1C) were instantly sampled at the time of retrieving the root bag from the soils to assess the effects of the rhizosphere on the microbial community. The soil genomic DNA extraction and next-generation DNA sequencing are detailed in the supplementary information. The 16S rRNA gene sequence data were deployed in NCBI GenBank (SUB8907191). The alpha and beta diversity analyses were performed in QIIME 1.8.0. Indices of Chao 1, Shannon, Simpson, and Good’s coverage were selected for the alpha diversity analysis. The beta diversity index and principal coordinates analysis (PCoA) were applied to calculate the differences between samples. The changes in the microbial community were further evaluated using linear discriminant analysis (LDA) effect size (LEfSe) (Gustave et al. 2019; Segata et al. 2011). In addition, high-throughput qPCR reactions were performed to identify As metabolic genes using Wafergen SmartChip Real-time reactions (Chen et al. 2016). Soil DNA was analyzed by high-throughput

qPCR AsChip as reported by Zhao et al. (2019). Nineteen As genes, including As(III) oxidation (*aoxA/B/C/D/R/S/aoxH*, and *arxA*), As(V) reduction (*arrA/B*, and *arsC/R*), As methylation and demethylation (*arsM* and *arsI*), and As transport (*arsA/B/D/P*, and *acr3*), were quantified.

Statistical analysis

The element information was extracted from the raw data files acquired by ICP-MS analysis using R software (version 3.5.0) (Yuan et al. 2019). In addition, R software was also used to plot the graphs. Data from different treatments were subjected to one-way analysis of variance (ANOVA) to determine statistical significance ($p < 0.05$) using SPSS 22 software (IBM SPSS, Armonk, NY, USA). For multielement comparisons and to indicate their differences in the root bag surroundings and in the bulk soils, their concentrations in 0-1.7, 1.7-3.4, 3.4-5.1, 5.1-6.8, 6.8-8.5, 8.5-10.2 mm and 10.2-22 mm distances were selected. Microbial variation in the 0-2 mm distance from the root bag between the treatment and control was compared to show the shift of the microbial community in the rhizosphere. The potential bias of the element supply from porewater to roots was calculated with ($Element_{10\text{-}22\ mm}$ - $Element_{0\text{-}1.7\ mm}$)/$Element_{0\text{-}1.7\ mm}$*100. Translocation coefficients of the element from the bulk soil to rhizosphere ($T_{bs\text{-}r}$), rhizosphere to root ($T_{r\text{-}r}$), root to stem ($T_{r\text{-}s}$), stem to leaf ($T_{s\text{-}l}$), and bulk soil to leaf ($T_{overall}$) were calculated with $Element_{0\text{-}1.7\ mm}/Element_{10\text{-}22\ mm}$, $Element_{root}/Element_{rhizosphere}$, ($Element_{stem}$ + $Element_{leaf}$)/($Element_{root}$ + $Element_{stem}$ + $Element_{leaf}$), $Element_{leaf}/(Element_{stem}$ + $Element_{leaf})$, and $Element_{leaf}/Element_{bulk\ soil}$, respectively.

Results

Spatiotemporal changes of multiple solute elements across the rhizosphere

In this study, the temporal-spatial variation in solute-phase elements across the rice rhizosphere was mapped at DAF 0, 3, 8, 15, 24, 30 and 40 with or without growing rice in the root bags. We monitored Fe, Mn, P, As, S, Cd, Sb, Cr, Co and Zn *in situ* across 0–22 mm from the root surface with a spatial resolution of 1.7 mm. Considerable temporal-spatial variation in the elements was observed across the rhizosphere (Fig. 2).

The solute-phase concentrations of the elements in bulk soil porewater varied with the flooding period and could be clustered into 3 groups, as shown in the control without growing rice in the root bags (Fig. S2). Group 1 includes Fe, Mn, P, As, S, and Co. In group 1, solute-phase Fe increased from 2.59 $mg{\cdot}L^{-1}$ at DAF 0 to a peak of 42.3 $mg{\cdot}L^{-1}$ at DAF 30 and then decreased to 15.9 $mg{\cdot}L^{-1}$ at DAF 40 (Fig. S2A). All the elements in group 1 shared a similar temporal pattern with Fe. Group 2 includes 2 elements (Cr and Zn), which also increased initially and dropped like group 1, but an increase of solute-phase Cr and Zn quickly started from DAF 3, and the high values were maintained for approximately one month before declining. Cd and Sb are the group 3. The elements in group 3 decreased rapidly after flooding (Fig.

S2G&F). Solute-phase Sb decreased dramatically from 74.6 $\mu g \cdot L^{-1}$ at DAF 0 to an average of 30.4 $\mu g \cdot L^{-1}$ after DAF 3 (Fig. S2G). More significantly, solute-phase Cd decreased approximately 10-fold after DAF 3 (1.45 $\mu g \cdot L^{-1}$) compared to that in DAF 0 (10.4 $\mu g \cdot L^{-1}$, Fig. S2G). The correlation analysis vividly demonstrates the covarying changes of the elements. Figure 1K&S2K illustrate that the changes in Fe, Mn, P, As, S, Cr, Co and Zn were not covaried with Cd and Sb, especially for Cd (r = -0.42), showing that the behaviors of the elements in group 3 were distinct from those in groups 1 and 2 (Fig. S2).

Rice roots have strong effects on the spatiotemporal changes in elements in the rhizosphere (Fig. 2). In the absence of rice roots, there was no apparent spatial pattern of those elements (Fig. S2). Solute-phase Fe, Mn, P, As, Co and Sb were immobilized in the presence of rice roots beginning at DAF 15 (Fig. 2A-D&I). During root development, the immobilization zone extended from 0–2 to 0–10 mm from the root, except for Sb. The immobilization of Sb only occurred < 2 mm from the roots. In contrast, solute-phase Cd and Zn were substantially promoted in the rhizosphere from DAF 8 (Fig. 2F&J). Additionally, the mobilization zone of Zn was much larger than that of Cd. The high Zn zone extended to 10 mm from the root, and the mobilization zone of Cd was restricted to < 2 mm. The roots had weak and insignificant effects on S and Cr (Fig. 2E&H).

Speciation of As and S across the rhizosphere and the driving factors

To interpret the potential biogeochemical mechanisms involved in regulating As and S redox in the rice rhizosphere, their speciation across the rhizosphere and associated driving factors were investigated. Among the common As and S species, only 2 As (As(V) and As(III)) and one S species (S(VI)) were detected in the soil porewater, while methyl As and S(-II) were not detected.

In the absence of rice roots, no apparent spatial pattern was observed for the As concentration and species across the rhizosphere. The sum of As(III) and As(V) remained at approximately 33.0 $\mu g \cdot L^{-1}$ in the soil porewaters, with an As(III) proportion of 67.6% (Fig. 3). In contrast, in the presence of rice roots, an obvious spatial pattern was detected for As across the rhizosphere. The sum of As(III) and As(V) decreased linearly from 40.5 $\mu g \cdot L^{-1}$ at > 10 mm from roots to as low as 5.93 $\mu g \cdot L^{-1}$ at 0–2 mm around the roots (Fig. 3). Moreover, the As(III) proportion increased from 65.6–89.2% with a decreasing distance from the roots. Figure 3 clearly illustrates that the rhizosphere retained a relatively high As(III) concentration, while As(V) was almost depleted within 0–4 mm around the roots. However, the presence or absence of rice roots had an insignificant effect on the S concentration and speciation across the rhizosphere. The S(VI) remained at approximately 180 $mg \cdot L^{-1}$ in the soil porewaters (Fig. 3).

Analysis of the 16S rRNA gene at 0–2 mm from the root bag yielded a high value of Good's coverage (> 0.96, Table S2), indicating that the sequencing was deep enough to cover the bacterial communities. Alpha analysis obtained similar Chao 1 (10253) and Shannon (6.73) values for all treatments. However, principal coordinates analysis of PCoA1 *vs.* PCoA2 (explaining 72.0%) showed that the bacterial communities were different between the two treatments (Fig. 4A). This indicates that growing rice could significantly alter the bacterial community in the rhizosphere. Furthermore, LEfSe analysis identified that

some bacterial groups, such as *Bacteroidetes*, *Proteobacteria*, *Acidobacteria*, and *Thiobacillus*, were enriched around the roots (Fig. S3).

To further reveal the potential involvement of biotic regulation of As in the rhizosphere, 19 As genes were investigated by AsChip analysis. In the absence of rice roots, *aoxB* and *arsC* were the most abundant As genes in the soils (Fig. 4B), while *aoxD* and *arsD* were undetectable. Our results suggested that growing rice significantly increased the abundance of all As(III)-oxidizing genes. This result indicates that biotic As oxidation could be substantially promoted by oxygenation of the rhizosphere via ROL. For As reduction, methylation, and transport, some of their genes were promoted in the rhizosphere, including *arsACIPR*.

Discussions

The element behaviors in the plant rhizosphere have received much attention due to their importance in plant nutrition. However, tracking their dynamic distributions in the rhizosphere is still challenging. A broad view of the spatiotemporal changes in elements in the rice rhizosphere is made possible by using Rhizon profilers.

The covariance of elements such as Fe, Mn, As, P, Co and S (Fig. 2) in time and space in the rhizosphere was mainly attributed to the adsorption sites provided by Fe oxides for the noted elements in the rhizosphere (Han et al. 2020; Ilhardt et al. 2019). Fe oxides serve as electron acceptors for dissimilatory Fe-reducing bacteria and are reduced under hypoxic conditions when soils are flooded (Zhang et al. 2012). Meanwhile, the solute-phase elements adsorbed on Fe oxides are re-immobilized by secondary Fe minerals (siderite, troilite, pyrite, and vivianite) after being released under continuous flooding (Borch et al. 2010; Burton et al. 2008; Muehe et al. 2019; Shaheen et al. 2013). Moreover, ROL-induced Fe plaques greatly enhanced the re-immobilization of solute-phase elements in the rice rhizosphere (Maisch et al. 2019). Consequently, the spatiotemporal fluctuation of aqueous Fe, Mn, P, As, S, and Co observed in this study could be well explained by the interplay between the mobilization and re-immobilization processes (Fig. 2). However, such detailed monitoring of multiple elements in the same rhizosphere has not yet been investigated. Previous studies generally reported only one-dimensional spatial or temporal changes in elements (Fulda et al. 2013; Jia et al. 2013, 2014; Muehe et al. 2019; Williams et al. 2014; Yin et al. 2020). In addition, two-dimensional changes in elements, such as with a limited spatial resolution (cm-scale with the Rhizon sampler) and/or measurement range (few parameters with planar optode), have also been previously documented (Bravin et al. 2008; Maisch et al. 2019). However, they failed to reveal the detailed spatiotemporal dynamics of multiple elements in the rhizosphere. The present study achieved this goal by providing an advanced solution by integrating/utilizing as many associated parameters as possible to deeply investigate element cycling in the rhizosphere.

The collection of fine-scale As species profiles in this study revealed that both As(III) and As(V) were fixed in the rice rhizosphere (Fig. 3). The depletion (~ 1.3 $\mu g \cdot L^{-1}$) of As(V) at 0–4 mm from the root surface was attributed to its stronger affinity to Fe oxides than As(III). The depletion of As(V) in this study was attributed to its direct adsorption on Fe plaques (Chen et al. 2005) and the transformation of As(III) to

less mobile As(V) followed by its fixation on Fe plaques (Tong et al. 2019). The latter process could be stimulated by both abiotic and biotic As(III) oxidation mediated by ROL and microbes, respectively (Awasthi et al. 2017; Tong et al. 2019). The biotic pathway was supported by the significant promotion of all As oxidizing genes in the rhizosphere (Fig. 4). Despite the presence of methylation genes (*arsM*), no methyl As was detected in the rhizosphere (Fig. 4) or in the plant tissues (Fig. S6). Previous studies reported that considerable methyl As (mainly DMA) accumulated in rice grains originated from the soil (Lomax et al. 2012; Šlejkovec et al. 2020), since rice plants cannot perform As methylation *in vivo*. A recent study reported that inorganic As was first methylated by S(VI)-reducing bacteria followed by rapid demethylation of methyl As produced by methanogenic archaea under highly reducing conditions during flooding (Chen et al. 2019). However, the conversion of S(VI) to S(-II) was not observed (Fig. 3), indicating that S(VI)-reducing bacteria were not activated in this study. Consequently, the absence of methyl As might be attributed to the lack of S(VI)-reducing bacteria or other anaerobic microbes processing *arsM* genes.

Conversely, aqueous Cd and Sb tended to be immobilized during flooding, and Cd was further remobilized around roots (Fig. 2). The rapid decline in Cd and Sb after flooding was attributed to the formation of CdS and Sb_2S_3 (Arsic et al. 2018; Fulda et al. 2013). However, this may not be the case in this study, as significant S(-II) was not detected in the porewater (Fig. 3). We can conclude that the reduction of S(VI) to S(-II) was not activated during the 40-day incubation, and our results are consistent with a previous report indicating that this phenomenon continued until 49 days after flooding (Burton et al. 2008). The occurrence of this phenomenon is most likely because S(VI) reduction is much less energy favorable than Fe oxide reduction (Borch et al. 2010). Changes in soil pH were reported to be the major factor governing Cd mobility (Wang et al. 2019). Elevated soil pH induced by Fe oxide reduction could inhibit Cd mobilization under flooding. However, the immobilization of Sb is credited to secondary Fe minerals formed under S(-II)-free reducing conditions (Burton et al. 2019). In contrast, the acidification of the rice rhizosphere, potentially caused by protons generated during Fe^{2+} oxidation and plant exudates (Maisch et al. 2019), could significantly enhance Cd mobilization, which could also be further enhanced by chelating complexes (small organic acids) released by roots (rhizodeposits) (Li et al. 2013). Rhizodeposits could also explain the Zn mobilization observed in this study (Fig. 2). Conversely, As was mostly controlled by the oxidation-mediated development of Fe plaques and was little affected by rhizosphere acidification or rhizodeposits (Bravin et al. 2008).

Fe plaques have a high affinity for multiple solutes and are believed to be an important barrier for element uptake and translocation from porewater to plants (Gao et al. 2006; Violante and Pigna 2002; Xu et al. 2017). Therefore, elements in porewater around roots should be used to estimate their supply potential for plants. However, considerable bias could be introduced if the elemental concentration in bulk soil porewater was utilized to estimate the supply potential. Fe, Mn, P, As, Sb and Co could be overestimated with a bias up to 17.5% – 196%, while Cd and Zn could be underestimated with a bias as high as -54.1% and – 27.0%, respectively (Table 1). Considering the significant variation in the elemental translocation coefficient from the bulk soil to the rhizosphere (T_{bs-r}, 0.342–2.38), a well-resolved rhizosphere is

essential to predict elemental translocation from rhizosphere to root (T_{r-r}, 6.78–43726), root to stem (T_{r-s}, 0.00975-1.65), stem to leaf (T_{s-l}, 0.241–1.29), and porewater to leaf ($T_{overall}$, 1.93–5875). However, the well-resolved rhizospheric effect was not taken into account in most previous studies on plant nutrition due to a lack of appropriate techniques (Kuzyakov and Razavi 2019; Muehe et al. 2019; Shaheen et al. 2014; Wan et al. 2019). DGT probes and laser-induced breakdown spectroscopy were applied to investigate the well-resolved elements in the rhizosphere (Ilhardt et al. 2019; Williams et al. 2014; Yin et al. 2020); however, they can only provide a snapshot at a certain time point. Snapshot information might be limited in predicting element translocation and accumulation in plants owing to fluctuations in the soil/rhizosphere environment during flooding/root elongation (Chen et al. 2019; Muehe et al. 2019). Rhizon profilers that are able to provide well-resolved temporal data across the rhizosphere during plant growth could be employed to fully address the aforementioned limitation.

Table 1
Translocation of multiple elements from bulk soil porewater to rice leaves

Elements†	Bulk soil porewater	Leaf	Translocation coefficient‡				
			T_{bs-r}	T_{r-r}	T_{r-s}	T_{s-l}	$T_{overall}$
Sb	36.7	70.8	0.700	57.9	0.0773	0.615	1.93
As	112	358	0.342	1354	0.00975	0.705	3.19
Fe	37.4	167	0.369	1150	0.0155	0.679	4.45
Co	48.1	249	0.852	125	0.0417	1.17	5.18
S	324	1692	0.914	6.78	0.653	1.29	5.22
Mn	7.79	266	0.789	33.7	1.55	0.829	34.2
Zn	2.45	111	1.37	301	0.154	0.707	45.2
Cr	7.57	646	1.01	4816	0.0173	1.02	85.3
Cd	0.538	2297	2.38	43726	0.171	0.241	4268
P	0.204	1197	0.440	11296	1.65	0.716	5875

† The units for Fe, Mn, P and S: $mg \cdot L^{-1}$ (porewater) and $mg \cdot kg^{-1}$ (plant tissues); the units of Sb, As, Co, Zn, Cr and Cd: $\mu g \cdot L^{-1}$ (porewater) and $\mu g \cdot kg^{-1}$ (plant tissues).

‡ Translocation coefficient describes element migration from soil porewater to fresh plant tissues. T_{bs-r}, T_{r-r}, T_{r-s}, T_{s-l} and $T_{overall}$ are translocation coefficients of the element from bulk soil to rhizosphere, rhizosphere to root, root to stem, stem to leaf, and bulk soil to leaf, respectively.

Conclusions

We found that elements in rice plants are taken up from soil porewater in the rhizosphere, which is temporally and spatially determined by multiple biogeochemical processes in soils as well as exudates from plant roots. This is a first attempt to demonstrate two-dimensional (time and space) co-distributions of multiple elements and their species across the paddy rhizosphere with an updated porewater sampler. In addition, the broad view of elemental behaviors from bulk porewater to rhizosphere and then to plant tissues was also illustrated for the first time by combining the collected microbial data with element translocation and accumulation in plants. Therefore, this study is a crucial step in understanding rhizosphere processes and in determining how multiple micro-cycles of elements react with each other, with the microbial community structure, and with rhizospheric effects.

Declarations

Acknowledgments

The National Science Foundation of China (41977320, 41571305) and Key Programme Special Fund of XJTLU (KSF-A-20) financially supported this work. We appreciate the outstanding laboratory support from Yi-Li Cheng, Xiao Zhou, Xiao-Yan Zhang, and Liang-Ping Long.

Conflicts of interest

The authors declare no financial conflict.

Data availability

The data from this study will be made available by the authors upon request.

Authors' contributions

Z.C., Z.Y., and W.G. designed research; Z.Y., W.G., and F.L. performed research; Z.C., Z.Y., S.T.A., J.B., R.S., and W.G. wrote the paper.

References

Afroz H, Su S, Carey MP, Meharg AA, Meharg C (2019) Inhibition of microbial methylation via arsM in the rhizosphere: arsenic speciation in the soil to plant continuum. Environ Sci Technol 53: 3451-3463.

Arsic M, Teasdale PR, Welsh DT, Johnston SG, Burton ED, Hockmann K, Bennett WW (2018) Diffusive gradients in thin films (DGT) reveals antimony and arsenic mobility differs in a contaminated wetland sediment during an oxic-anoxic transition. Environ Sci Technol 52: 1118-1127.

Awasthi S, Chauhan R, Srivastava S, Tripathi RD (2017) The journey of arsenic from soil to grain in rice. Front Plant Sci 8: 1007.

Borch T, Kretzschmar R, Kappler A, Cappellen PV, Gindervogel M, Voegelin A, Campbell K (2010) Biogeochemical redox processes and their impact on contaminant dynamics. Environ Sci Technol 44: 15-23.

Brackin R, Atkinson BS, Sturrock CJ, Rasmussen A (2017) Roots-eye view: Using microdialysis and microCT to non-destructively map root nutrient depletion and accumulation zones. Plant Cell Environ 40: 3135-3142.

Bravin MN, Travassac F, Le Floch M, Hinsinger P, Garnier J-M (2008) Oxygen input controls the spatial and temporal dynamics of arsenic at the surface of a flooded paddy soil and in the rhizosphere of lowland rice (*Oryza sativa* L.): a microcosm study. Plant soil 312: 207-218.

Burton ED, Bush RT, Sullivan LA, Johnston SG, Hocking RK (2008) Mobility of arsenic and selected metals during re-flooding of iron- and organic-rich acid-sulfate soil. Chem Geol 253: 64-73.

Burton ED, Hockmann K, Karimian N, Johnston SG (2019) Antimony mobility in reducing environments: The effect of microbial iron (III)-reduction and associated secondary mineralization. Geochim Cosmochim Ac 245: 278-289.

Chen C, Li L, Huang K, Zhang J, Xie WY, Lu Y, Dong X, Zhao FJ (2019) Sulfate-reducing bacteria and methanogens are involved in arsenic methylation and demethylation in paddy soils. ISME J 13: 2523-2535.

Chen Q, An X, Li H, Su J, Ma Y, Zhu Y (2016) Long-term field application of sewage sludge increases the abundance of antibiotic resistance genes in soil. Environ Int 92: 1-10.

Chen Z, Huang YC, Liang JH, Zhao F, Zhu YG (2012) A novel sediment microbial fuel cell with a biocathode in the rice rhizosphere. Bioresource Technol 108: 55-59.

Chen Z, Zhu YG, Liu WJ, Meharg AA (2005) Direct evidence showing the effect of root surface iron plaque on arsenite and arsenate uptake into rice (*Oryza sativa*) roots. New Phytol 165: 91-97.

Eberle A, Besold J, Kerl CF, Lezama-Pacheco JS, Fendorf S, Planer-Friedrich B (2020) Arsenic fate in peat controlled by the pH-dependent role of reduced sulfur. Environ Sci Technol 54: 6682-6692.

Fulda B, Voegelin A, Kretzschmar R (2013) Redox-controlled changes in cadmium solubility and solid-phase speciation in a paddy soil as affected by reducible sulfate and copper. Environ Sci Technol 47: 12775-12783.

Gao Y, Leermakers M, Gabelle C, Divis P, Billon G, Ouddane B, Fischer JC, Wartel M, Baeyens W (2006) High-resolution profiles of trace metals in the pore waters of riverine sediment assessed by DET and DGT. Sci Total Environ 362: 266-277.

Guo T, Gustave W, Lu H, He Y, Tang X, Buchwalter DB, Xu J (2020) Periphyton enhances arsenic release and methylation at the soil-water interface of paddy soils. J Hazard Mater: 124946.

Gustave W, Yuan ZF, Ren YX, Sekar R, Chen Z (2019) Arsenic alleviation in rice by using paddy soil microbial fuel cells. Plant Soil 441: 111-127.

Han J, Kim M, Ro HM (2020) Factors modifying the structural configuration of oxyanions and organic acids adsorbed on iron (hydr)oxides in soils. A review. Environ Chem Lett 18: 631-662.

Hansel CM, Fendorf S, Sutton S, Newville M (2001) Characterization of Fe plaque and associated metals on the roots of mine-waste impacted aquatic plants. Environ Sci Technol 35: 3863-3868.

Ilhardt PD, Nuñez JR, Denis EH, Rosnow JJ, Krogstad EJ, Renslow RS, Moran JJ (2019) High-resolution elemental mapping of the root-rhizosphere-soil continuum using laser-induced breakdown spectroscopy (LIBS). Soil Biol Biochem 131: 119-132.

Jia Y, Huang H, Chen Z, Zhu YG (2014) Arsenic uptake by rice is influenced by microbe-mediated arsenic redox changes in the rhizosphere. Environ Sci Technol 48: 1001-1007.

Jia Y, Huang H, Zhong M, Wang FH, Zhang LM, Zhu YG (2013) Microbial arsenic methylation in soil and rice rhizosphere. Environ Sci Technol 47: 3141-3148.

Kumarathilaka P, Seneweera S, Meharg A, Bundschuh J (2018) Arsenic speciation dynamics in paddy rice soil-water environment: sources, physico-chemical, and biological factors-a review. Water Res 140: 403-414.

Kuzyakov Y, Razavi BS (2019) Rhizosphere size and shape: Temporal dynamics and spatial stationarity. Soil Biol Biochem 135: 343-360.

Li T, Tao Q, Liang C, Shohag MJI, Yang X, Sparks DL (2013) Complexation with dissolved organic matter and mobility control of heavy metals in the rhizosphere of hyperaccumulator Sedum alfredii. Environ Pollut 182: 248-255.

Liu HJ, Zhang JL, Zhang FS (2007) Role of iron plaque in Cd uptake by and translocation within rice (*Oryza sativa* L.) seedlings grown in solution culture. Environ Exp Bot 59: 314-320.

Lomax C, Liu W, Wu L, Xue K, Xiong J, Zhou J, McGrath SP, Meharg AA, Miller AJ, Zhao F (2012) Methylated arsenic species in plants originate from soil microorganisms. New Phytol 193: 665-672.

Ma X, Liu J, Wang M (2012) Differences between rice cultivars in iron plaque formation on roots and plant lead tolerance. Adv J Food Sci Technol 5: 160-163.

Maisch M, Lueder U, Kappler A, Schmidt C (2019) Iron lung: how rice roots induce iron redox changes in the rhizosphere and create niches for microaerophilic Fe (II)-oxidizing bacteria. Environ Sci Technol Lett 6:

600-605.

Martin BC, Bougoure J, Ryan MH, Bennett WW, Colmer TD, Joyce NK, Olsen YS, Kendrick GA (2019) Oxygen loss from seagrass roots coincides with colonisation of sulphide-oxidising cable bacteria and reduces sulphide stress. ISME J 13: 707.

Muehe EM, Wang T, Kerl CF, Planer-Friedrich B, Fendorf S (2019) Rice production threatened by coupled stresses of climate and soil arsenic. Nat Commun 10: 1-10.

Pester M, Knorr KH, Friedrich MW, Wagner M, Loy A (2012) Sulfate-reducing microorganisms in wetlands–fameless actors in carbon cycling and climate change. Front Microbiol 3: 72.

Quaghebeur M, Rengel Z, Smirk M (2003) Arsenic speciation in terrestrial plant material using microwave-assisted extraction, ion chromatography and inductively coupled plasma mass spectrometry. J Anal Atom Spectrom 18: 128-134.

Revsbech NP, Pedersen O, Reichardt W, Briones A (1999) Microsensor analysis of oxygen and pH in the rice rhizosphere under field and laboratory conditions. Biol Fertil Soils 29: 379-385.

Richardson AE, Barea JM, McNeill AM, Prigent Combaret C (2009) Acquisition of phosphorus and nitrogen in the rhizosphere and plant growth promotion by microorganisms. Plant Soil 321: 305-339.

Seeberg-Elverfeldt J, Schlüter M, Feseker T, Kölling M (2005) Rhizon sampling of porewaters near the sediment-water interface of aquatic systems. Limnol Oceanogr-Meth 3: 361-371.

Segata N, Izard J, Waldron L, Gevers D, Miropolsky L, Garrett WS, Huttenhower C (2011) Metagenomic biomarker discovery and explanation. Genome Biol 12: R60.

Shaheen SM, Rinklebe J, Rupp H, Meissner R (2014) Temporal dynamics of pore water concentrations of Cd, Co, Cu, Ni, and Zn and their controlling factors in a contaminated floodplain soil assessed by undisturbed groundwater lysimeters. Environ Pollut 191: 223-231.

Shaheen SM, Tsadilas CD, Rinklebe J (2013) A review of the distribution coefficients of trace elements in soils: Influence of sorption system, element characteristics, and soil colloidal properties. Adv Colloid Interface 201: 43-56.

Šlejkovec Z, Gorše L, Grobler A, Jagodic M, Falnoga I (2020) Arsenic speciation and elemental composition of rice samples from the Slovenian market. Food Chem: 128348.

Suda A, Makino T (2016) Functional effects of manganese and iron oxides on the dynamics of trace elements in soils with a special focus on arsenic and cadmium: A review. Geoderma 270: 68-75.

Suzuki Y, Shimoda Y, Endo Y, Hata A, Yamanaka K, Endo G (2009) Rapid and effective speciation analysis of arsenic compounds in human urine using anion-exchange columns in HPLC-ICP-MS. J Occup Health

51: 380-385.

Thomas F, Giblin AE, Cardon ZG, Sievert SM (2014) Rhizosphere heterogeneity shapes abundance and activity of sulfur-oxidizing bacteria in vegetated salt marsh sediments. Front Microbiol 5.

Tong H, Liu C, Hao L, Swanner ED, Chen M, Li F, Xia Y, Liu Y, Liu Y (2019) Biological Fe(II) and As(III) oxidation immobilizes arsenic in micro-oxic environments. Geochim Cosmochim Ac 265: 96-108.

Violante A, Pigna M (2002) Competitive sorption of arsenate and phosphate on different clay minerals and soils. Soil Sci Soc Am J 66: 1788-1796.

Wan Y, Huang Q, Camara AY, Wang Q, Li H (2019) Water management impacts on the solubility of Cd, Pb, As, and Cr and their uptake by rice in two contaminated paddy soils. Chemosphere 228: 360-369.

Wang J, Wang PM, Gu Y, Kopittke PM, Zhao FJ, Wang P (2019) Iron–manganese (oxyhydro)oxides, rather than oxidation of sulfides, determine mobilization of Cd during soil drainage in paddy soil systems. Environ Sci Technol 53: 2500-2508.

Williams PN, Santner J, Larsen M, Lehto NJ, Oburger E, Wenzel W, Glud RN, Davison W, Zhang H (2014) Localized flux maxima of arsenic, lead, and iron around root apices in flooded lowland rice. Environ Sci Technol 48: 8498-8506.

Xu B, Yu S, Ding J, Wu S, Ma J (2015) Metal-dependent root iron plaque effects on distribution and translocation of chromium and nickel in yellow flag (*Iris pseudacorus* L.). Int J Phytoremediat 17: 175-181.

Xu X, Chen C, Wang P, Kretzschmar R, Zhao FJ (2017) Control of arsenic mobilization in paddy soils by manganese and iron oxides. Environ Pollut 231: 37-47.

Ye ZH, Cheung KC, Wong MH (2001) Copper uptake in *Typha latifolia* as affected by iron and manganese plaque on the root surface. Can J Botany 79: 314-320.

Yin DX, Fang W, Guan DX, Williams PN, Moreno Jimenez E, Gao Y, Zhao FJ, Ma LQ, Zhang H, Luo J (2020) Localized intensification of arsenic release within the emergent rice rhizosphere. Environ Sci Technol 54: 3138-3147.

Yuan ZF, Gustave W, Boyle J, Sekar R, Bridge J, Ren Y, Tang X, Guo B, Chen Z (2020) Arsenic behavior across soil-water interfaces in paddy soils: coupling, decoupling and speciation. Chemosphere: 128713.

Yuan ZF, Gustave W, Bridge J, Liang Y, Sekar R, Boyle J, Jin CY, Pu TY, Ren YX, Chen Z (2019) Tracing the dynamic changes of element profiles by novel soil porewater samplers with ultralow disturbance to soil–water interface. Environ Sci Technol 53: 5124-5132.

Yuan ZF, Gustave W, Sekar R, Bridge J, Wang JY, Feng WJ, Guo B, Chen Z (2021) Simultaneous measurement of aqueous redox-sensitive elements and their species across the soil-water interface. J Environ Sci 102: 1-10.

Zhang C, Ge Y, Yao H, Chen X, Hu M (2012) Iron oxidation-reduction and its impacts on cadmium bioavailability in paddy soils: a review. Front Envi Sci Eng 6: 509-517.

Zhang X, Zhang F, Mao D (1999) Effect of iron plaque outside roots on nutrient uptake by rice (*Oryza sativa* L.): Phosphorus uptake. Plant Soil 209: 187-192.

Zhao Y, Su J, Ye J, Rensing C, Tardif S, Zhu Y, Brandt KK (2019) AsChip: a high-throughput qPCR chip for comprehensive profiling of genes linked to microbial cycling of arsenic. Environ Sci Technol 53: 798-807.

Figures

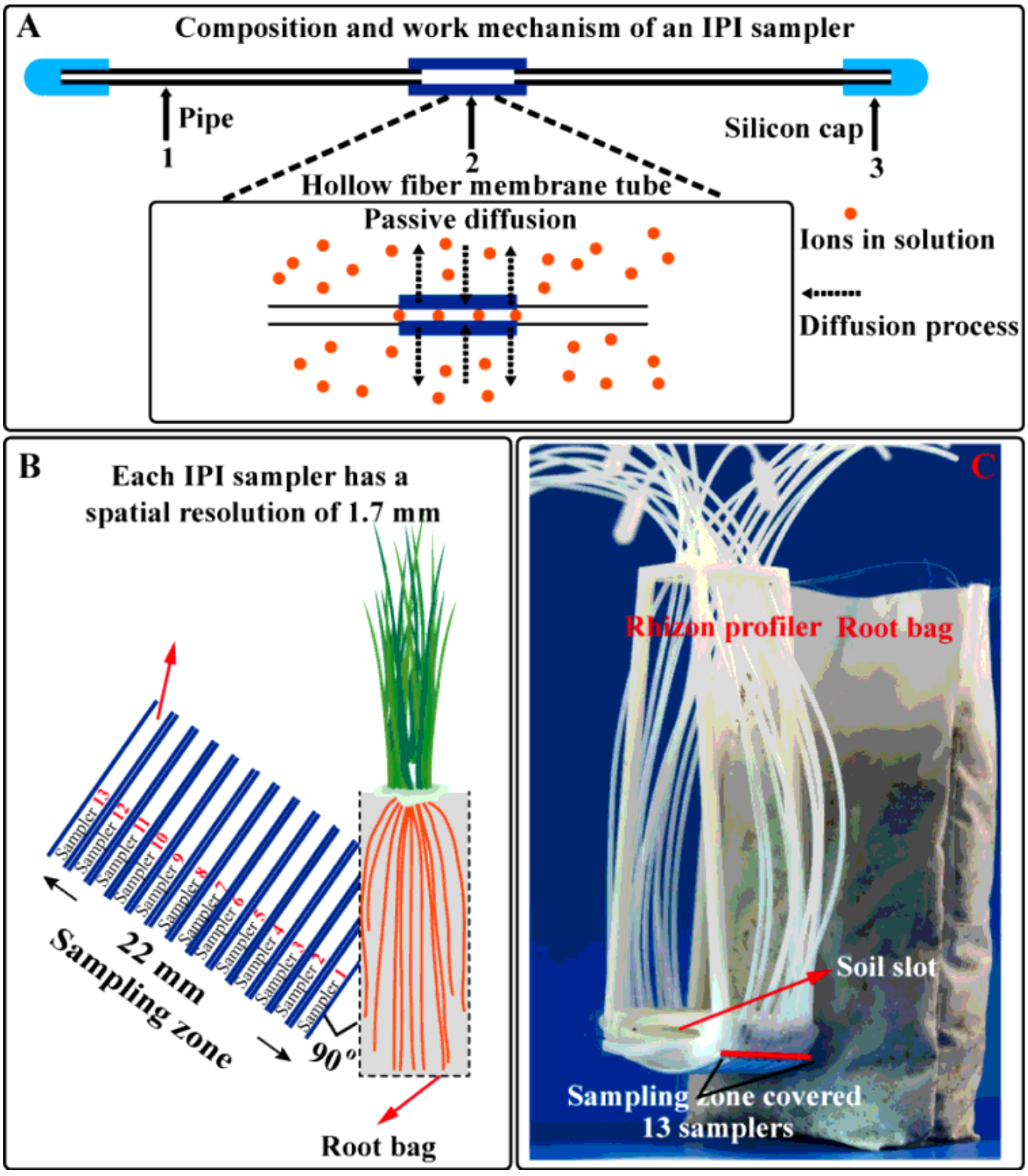

Figure 1

Porewater across the rice rhizosphere sampled by 13 In-situ Porewater Iterative (IPI) samplers assembled in each Rhizon profiler. A) A typical IPI sampler; B) conceptual diagram of using an IPI sampler array to sample porewaters across the rice rhizosphere; C) real photo of the IPI array, i.e., Rhizon profiler combined with a root bag.

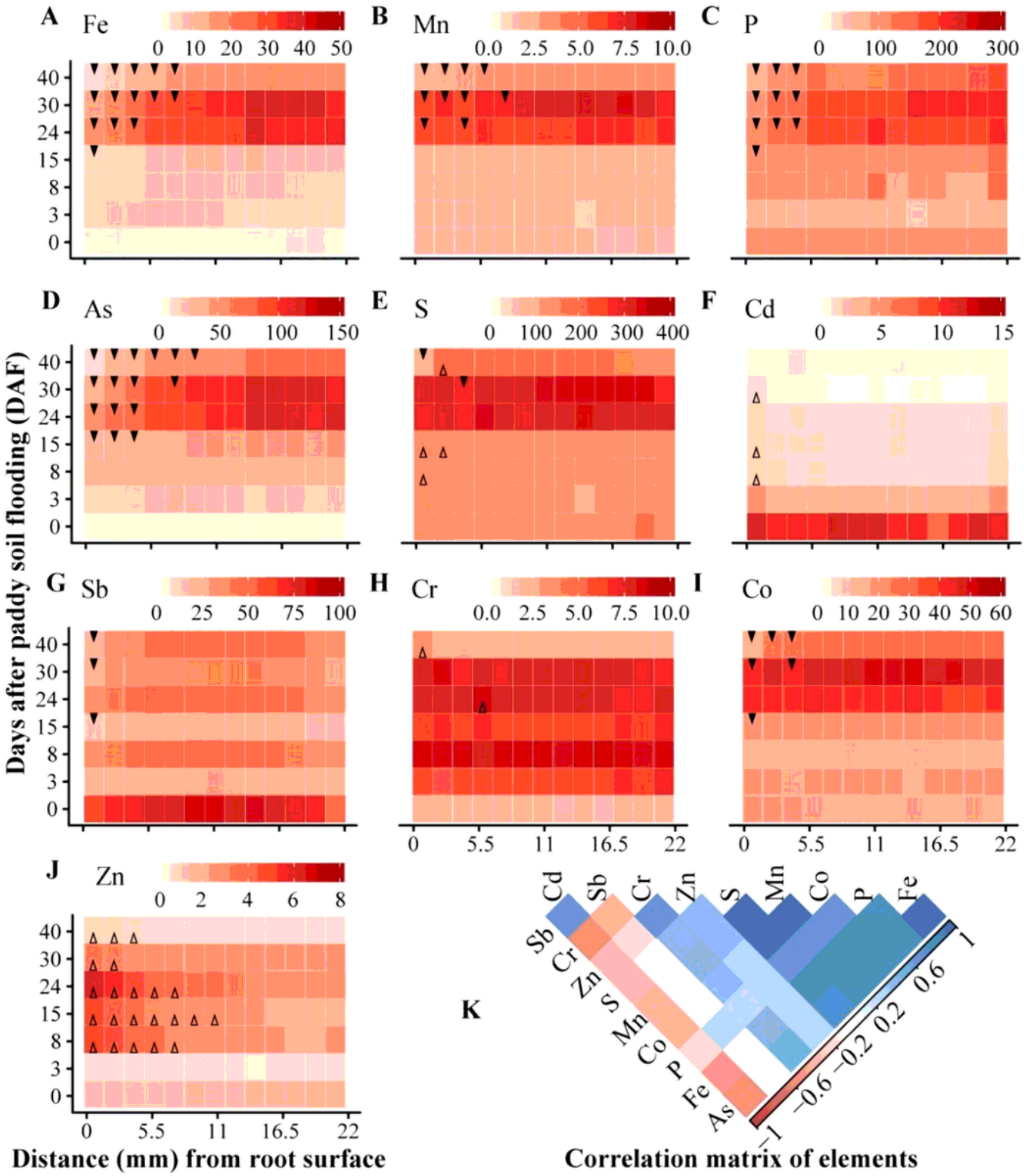

Figure 2

Profiles of multiple elements across the rhizosphere at days after paddy soil flooding (DAF) 0-40 with rice growing in root bags. A-J: Heatmaps of Fe (mg·L-1, A), Mn (mg·L-1, B), P (μg·L-1, C), As (μg·L-1, D), S (mg·L-1, E), Cd (μg·L-1, F), Sb (μg·L-1, G), Cr (μg·L-1, H), Co (μg·L-1, I), Zn (μg·L-1, J), with the down-direction solid triangle and up-direction hollow triangle indicating significantly lower or higher,

respectively, compared to that of the control group ($p < 0.05$, n = 3). K: Correlation matrix of elements in the rhizosphere (0-10.2 mm, n = 147).

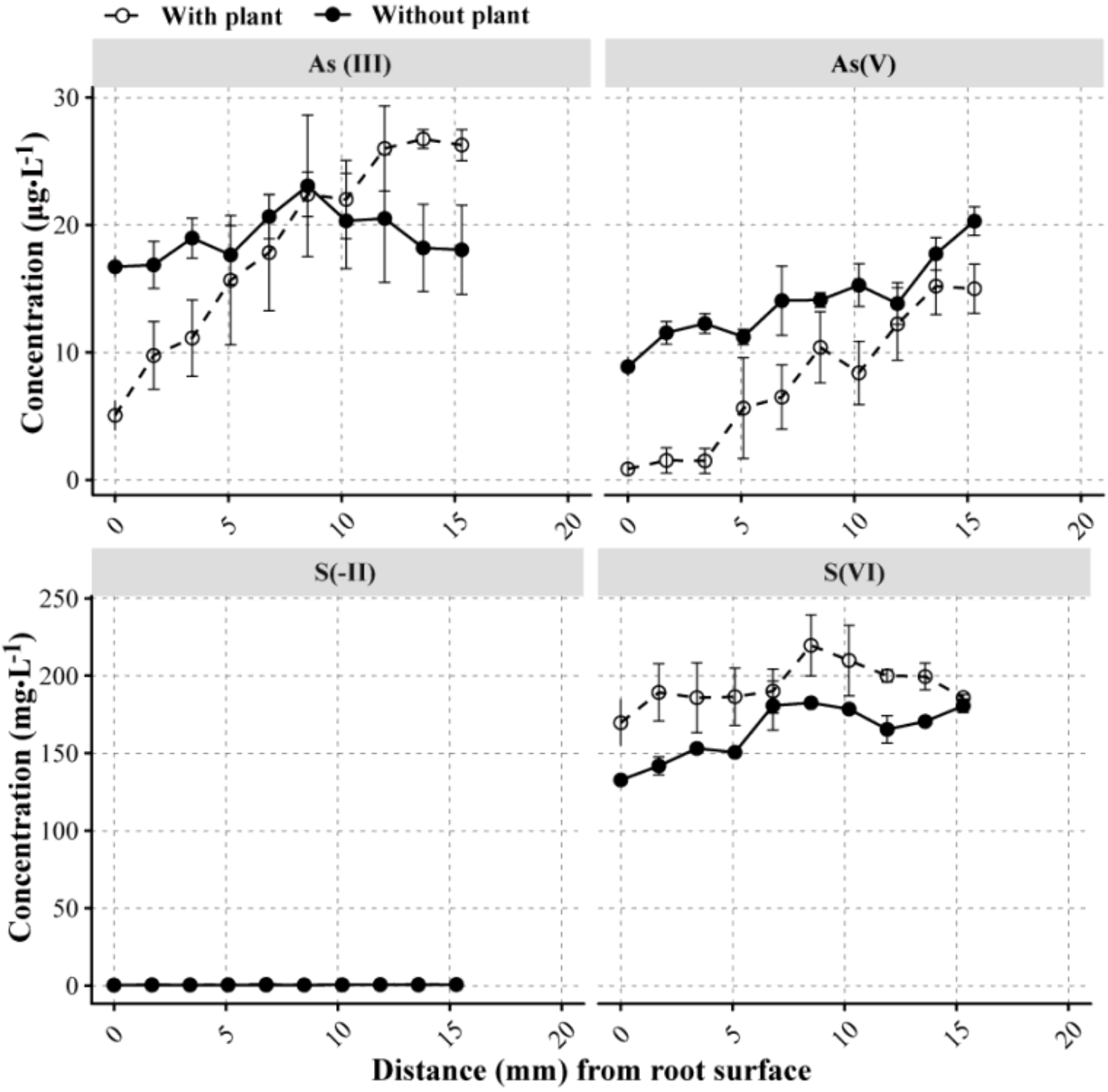

Figure 3

Spatial changes in As and S species across the rhizosphere (0-15 mm) at DAF 40. Arsenic and S species include arsenite [As(III)] and arsenate [As(V)] and sulfide [S(-II)] and sulfate [S(VI)], respectively. S(-II) was not detected.

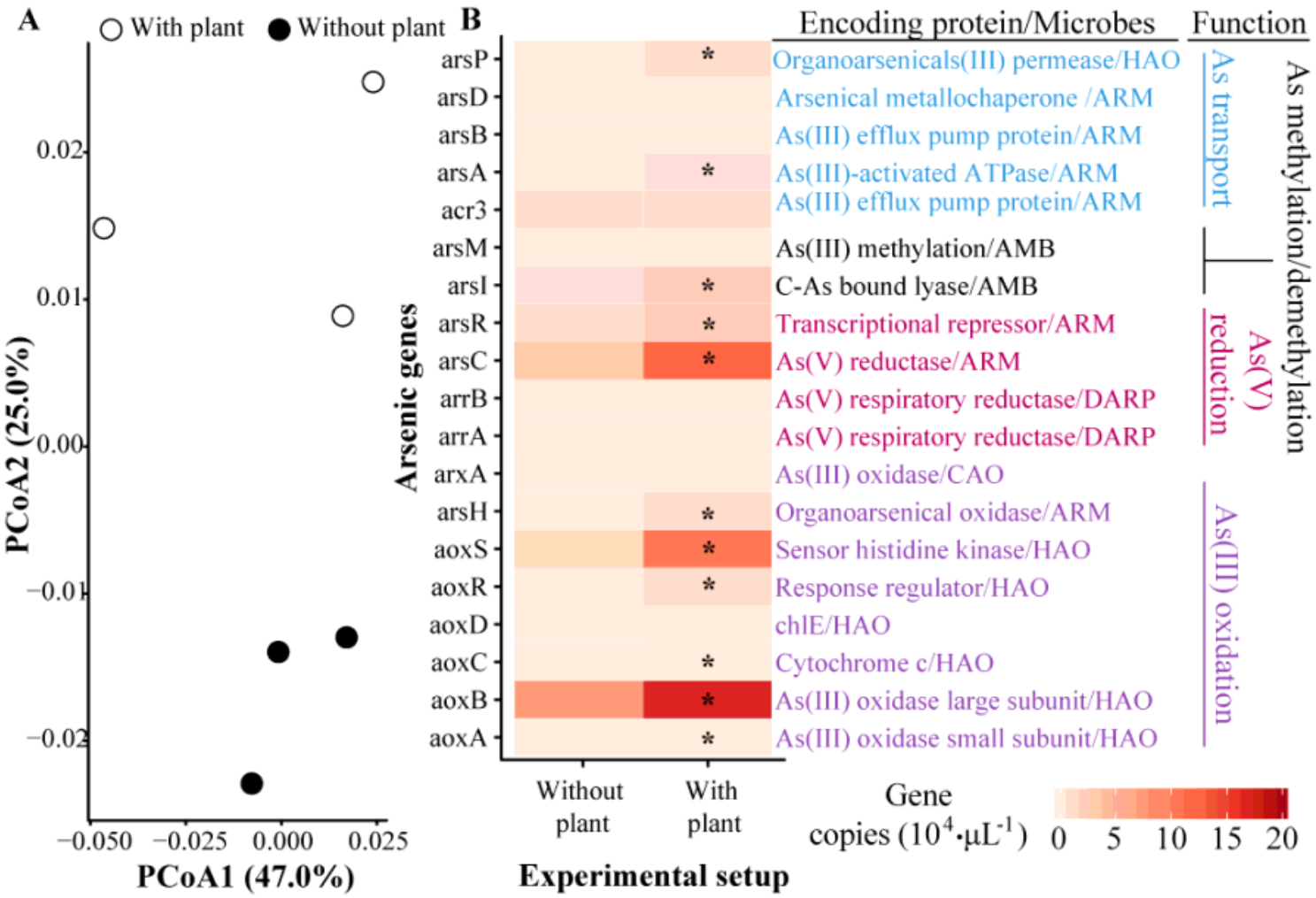

Figure 4

Principal coordinates analysis (PCoA) of the microbial community (A) and the abundances of 19 As genes (B) around root bags at DAF 40. Abbreviations used: HAO, heterotrophic As(III) oxidizers; ARM, As-resistant microorganisms; CAO, chemoautotrophic As(III) oxidizers; DARP, dissimilatory As(V)-reducing prokaryotes. The star represents significance ($p < 0.05$).

Supplementary Files

This is a list of supplementary files associated with this preprint. Click to download.

- IPI4SI.pdf